Simultaneous retrieval of atmospheric CO_2 and light path modification from space-based spectroscopic observations of greenhouse gases: methodology and application to GOSAT measurements over TCCON sites

Sergey Oshchepkov,[1,*] Andrey Bril,[1] Tatsuya Yokota,[1] Yukio Yoshida,[1] Thomas Blumenstock,[2] Nicholas M. Deutscher,[3,4] Susanne Dohe,[2] Ronald Macatangay,[4] Isamu Morino,[1] Justus Notholt,[3] Markus Rettinger,[5] Christof Petri,[3] Matthias Schneider,[2] Ralf Sussman,[5] Osamu Uchino,[1] Voltaire Velazco,[4] Debra Wunch,[6] and Dmitry Belikov[1]

[1]Center for Global Environmental Research, National Institute for Environmental Studies, 16-2 Onogawa, Tsukuba, Ibaraki 305-8506, Japan

[2]Karlsruhe Institute of Technology (KIT), IMK ASF, Leopoldshafen 76344, Germany

[3]Institute of Environmental Physics, University of Bremen, Otto-Hahn-Allee 1, Bremen D-28334, Germany

[4]Centre for Atmospheric Chemistry, School of Chemistry, University of Wollongong, Northfields Avenue, NSW 2522, Australia

[5]Karlsruhe Institute of Technology (KIT), IMK-IFU, Garmisch-Partenkirchen 82467, Germany

[6]131-24, Geological and Planetary Sciences Division, California Institute of Technology, 1200 E California Blvd., Pasadena, California 91125, USA

*Corresponding author: sergey.oshchepkov@nies.go.jp

Received 18 October 2012; revised 23 December 2012; accepted 25 December 2012; posted 23 January 2013 (Doc. ID 178308); published 19 February 2013

This paper presents an improved photon path length probability density function method that permits simultaneous retrievals of column-average greenhouse gas mole fractions and light path modifications through the atmosphere when processing high-resolution radiance spectra acquired from space. We primarily describe the methodology and retrieval setup and then apply them to the processing of spectra measured by the Greenhouse gases Observing SATellite (GOSAT). We have demonstrated substantial improvements of the data processing with simultaneous carbon dioxide and light path retrievals and reasonable agreement of the satellite-based retrievals against ground-based Fourier transform spectrometer measurements provided by the Total Carbon Column Observing Network (TCCON).

OCIS codes: 280.4991, 010.5620, 300.6320, 290.1090.

1. Introduction

Space-based global observations of carbon dioxide (CO_2) from passive remote sensing of upwelling solar electromagnetic radiation are recognized as being important for improving our understanding of the spatial and temporal distributions of CO_2 in the atmosphere. The Japanese Greenhouse gases Observing SATellite "IBUKI" (GOSAT), in orbit since 23 January 2009, is the world's first satellite mission dedicated to measuring the concentrations of CO_2

1559-128X/13/061339-12$15.00/0

and methane from space. The on-board Fourier transform spectrometer (FTS) provides high-resolution spectroscopic measurements of light reflected and emitted from the Earth's surface and the atmosphere in the short-wave infrared and thermal infrared spectral range [1–3].

Estimation of the column-averaged gas amounts from such satellite-based measurements is an extremely challenging task because the requirements on the retrieval accuracy are rather stringent. For example, several theoretical studies have shown that a precision of ~1.5 parts in 10^6 (ppm) or better for monthly mean column-averaged dry air mole fractions of CO_2 (X_{CO2}) on a regional scale with sub-ppm bias is required to constrain uncertainties in surface CO_2 fluxes derived from *in situ* measurements (e.g., [4–7]). The major source of error in space-based retrieval of gas amounts is the modification of the light path due to atmospheric light scattering. A number of studies [8–15] have shown that, even under clear sky conditions, high-altitude subvisible cirrus or elevated aerosols can introduce large latitudinal/spatial and/or temporal biases in gas retrievals, which could hamper CO_2 surface flux inversions.

To provide highly accurate retrievals of the atmospheric gas abundances, several algorithms have been developed in different groups throughout the world to process the GOSAT data [13–22]. These algorithms have been outlined in [23]. Reference [23] also provides algorithm cross comparison when retrieving column-averaged CO_2 abundance as well as compares the retrievals from different algorithms with the ground-based FTS observations from the Total Carbon Column Observing Network (TCCON) [24].

This paper focuses on further developments of the photon path length probability density function (PPDF) method toward simultaneous gas and optical path retrievals, which allows for satellite data processing under non-negligible light path modification.

The PPDF-based method [13,14,16] accounts for atmospheric light scattering through light path modification, which can be examined using the photon path length statistical characteristics and the equivalence theorem [25]. This method allows for rapid radiative transfer spectral calculations in the data processing because the light path modification is similar within each individual GOSAT band. In our previous version of the PPDF-based algorithm, the retrieval of PPDF parameters was used as a prescreening step to identify satellite soundings that are not distinctly affected by atmospheric light scattering. These near clear sky soundings are recognized by low values of PPDF parameters retrieved from radiance spectra in the molecular oxygen (O_2) A-band at 0.76 μm. The retrieval of gas amounts is then carried out from radiance spectra in the near-infrared CO_2 and CH_4 bands assuming zero optical path modification. As discussed elsewhere [13], the retrieval scheme with this assumption is conducted on the basis of differential optical absorption spectroscopy (DOAS) [26,27]. We refer to this method as PPDF-D [18]. This method showed reasonable agreement in CO_2 retrievals as compared with ground-based X_{CO2} measurements over TCCON sites [18] and other retrieval algorithms [23]. Unfortunately, the number of observations accessible to the processing was rather limited. This paper aims to develop an improved PPDF-based version that simultaneously retrieves gas column abundance and the optical path. We will refer to this method as PPDF-S. PPDF-S retrievals substantially increase the amount of observation data applicable for accurate gas retrievals. This is made possible by processing additional satellite observations for which the light path modifications due to atmospheric light scattering by aerosol and clouds are not negligible.

The paper is organized as follows. Section 2 introduces the methodology for simultaneous gas and light path retrievals. In Section 3, we briefly outline the FTS measurements from GOSAT and TCCON used in this study for the data processing and validation of the retrievals. Section 4 describes the results of GOSAT data processing and compares the retrievals with TCCON measurements. We also include two other algorithms in the GOSAT–TCCON X_{CO2} comparison. Section 5 summarizes the results.

2. Methodology

A. Inversion Scheme

To process the radiance spectra provided by the space-based measurements, we apply the maximum *a posteriori* rule

$$\hat{\boldsymbol{x}} = \underset{\boldsymbol{x}}{\operatorname{argmin}}\{\chi^2(\boldsymbol{R}^*, \boldsymbol{x}_a, \boldsymbol{x})\} \tag{1}$$

to minimize the weighed least-squares deviation between measured $\boldsymbol{R}^*$ and modeled $\boldsymbol{R}'(\boldsymbol{x})$ radiance spectra with the available *a priori* data $\boldsymbol{x}_a$ for the desired state vector $\boldsymbol{x}$:

$$\chi^2(\boldsymbol{R}^*, \boldsymbol{x}_a, \boldsymbol{x}) = \|\boldsymbol{R}^* - \boldsymbol{R}'(\boldsymbol{x})\|^2_{C_R} + \|\boldsymbol{x}_a - \boldsymbol{x}\|^2_{C_a}. \tag{2}$$

In Eq. (2) the state vector $\boldsymbol{x}$ includes CO_2 concentration vertical profiles $x_{CO2}(h)$; the squared norms

$$\|z\|^2_C = z^T \boldsymbol{C}^{-1} z \tag{3}$$

are weighted by covariance matrices of measurement errors of $\boldsymbol{R}^*$ ($\boldsymbol{C}_R$) and of *a priori* assumptions $\boldsymbol{x}_a$ ($\boldsymbol{C}_a$). The measurement vector $\boldsymbol{R}^*$ corresponds to a set of M spectral channels $\Delta\nu_m$ ($m = 1, 2, \ldots M$) within which the modeled radiance $\boldsymbol{R}'(\boldsymbol{x})$ is convolved using the instrumental line-shape (ILS) function.

Different algorithms for satellite data processing are mainly distinguished by the radiative transfer forward model [$\boldsymbol{R}'(\boldsymbol{x})$] and by the content of the state vector $\boldsymbol{x}$. The PPDF-based methods deal with representation of the modeled radiance spectra through the effective transmittance $\tilde{T}_\nu(\boldsymbol{x})$:

$$\ln R'_{\Delta\nu_m} = \ln \langle S_\nu^0 \tilde{T}_\nu(x) \rangle_{\Delta\nu_m} - P_{\Delta\nu_m}. \quad (4)$$

In Eq. (4) $P_{\Delta\nu_m}$ is a spectral polynomial of low order designed to remove the low-frequency portion of the processed spectra in the retrieval process. This portion could be associated with light scattering by near-ground aerosols or spectral variability in surface albedo [13]. Solar irradiance S_ν^0 and the effective transmittance $\tilde{T}_\nu(x)$ spectra in Eq. (4) are convolved using the ILS within each channel $\Delta\nu_m$. Note that the GOSAT ILS could result in negative radiance values for strongly saturated absorption lines. These negative data were present in minor amounts and were excluded from the retrieval procedure when fitting the logarithm of radiance by using Eq. (4). Under negligible atmospheric light scattering the effective transmittance

$$\tilde{T}_\nu\{x(h)\} = \exp\{-A_G \tau_g\} \quad (5)$$

depends on the gas optical depth $\tau_g = \int_0^{h_A} k(h)\mathrm{d}h$ and geometric air-mass factor $A_G = \big((1/\cos\Theta) + (1/\cos\Theta_0)\big)$, where Θ and Θ_0 are the solar zenith angle and the ray incident angle to the satellite, respectively, h_A is the altitude at the top of the atmosphere, $k(h) = x_{CO2}(h)\zeta(h)$ is the gas absorption coefficient, and $\zeta(h)$ is the gas cross section. To account for the atmospheric light scattering by aerosols and subvisible clouds, the effective transmittance $\tilde{T}$ was additionally expressed through a set of PPDF parameters describing the effects of the optical path ($A_G\tau_g$) modification [13,16]. Two basic parameters are involved to account for optical path modification. One describes optical path shortening (α), and another (ρ) describes light path lengthening compared with the direct nonperturbed path from the Sun to the surface to the satellite:

$$\bar{L} = \left(\frac{1}{\cos\Theta} + \frac{1}{\cos\Theta_0}\right) h_A. \quad (6)$$

In our previous version of the PPDF-based algorithm (PPDF-D), the retrieval of PPDF parameters was used as a prescreening step to identify satellite soundings that are not distinctly affected by atmospheric light scattering. These clear sky soundings are indicated by low values of PPDF parameters ($\alpha \le 0.04$, $\rho \le 0.04$) retrieved from radiance spectra in the molecular O_2 A-band at 0.76 μm when the optical path modification is therefore assumed to be negligible in the CO_2 absorption bands at 1.6 and 2.0 μm [28]. Then the retrieval of gas amounts is performed from radiance spectra in the gas bands with zero optical path modification using Eq. (4). As discussed earlier [13], the retrieval scheme with this assumption is conducted on the basis of DOAS [26,27].

This method (PPDF-D) showed reasonable agreement of CO_2 retrievals with those from ground-based TCCON measurements [18], but the number of observations is rather limited [23] due to restriction to very clear sky conditions where the light path modification is negligible. Another drawback of PPDF-D is that the retrieved PPDF parameters in O_2 A-band are not always appropriate for characterizing the light path modification in the target CO_2 absorption bands. This effect can be minimized by limiting the difference in ground surface albedo between the bands [23]. Unfortunately, this restriction results in further reduction of the GOSAT data adaptable for the processing, especially for bright surfaces such as over the Sahara or Australian deserts [23].

In this paper, we improve the PPDF-based method toward simultaneous gas and optical path retrievals using high-resolution spectroscopic observations in three short-wave infrared bands at 0.76, 1.6, and 2.0 μm (PPDF-S). This permits satellite data processing under non-negligible light path modification, thereby substantially increasing the number of observations available for the data processing with accurate gas retrievals due to light path correction. Figure 1 presents a simplified flow chart of the data processing.

Three-band simultaneous gas and light path retrievals require an accurate representation of Rayleigh light scattering through the atmosphere [mostly

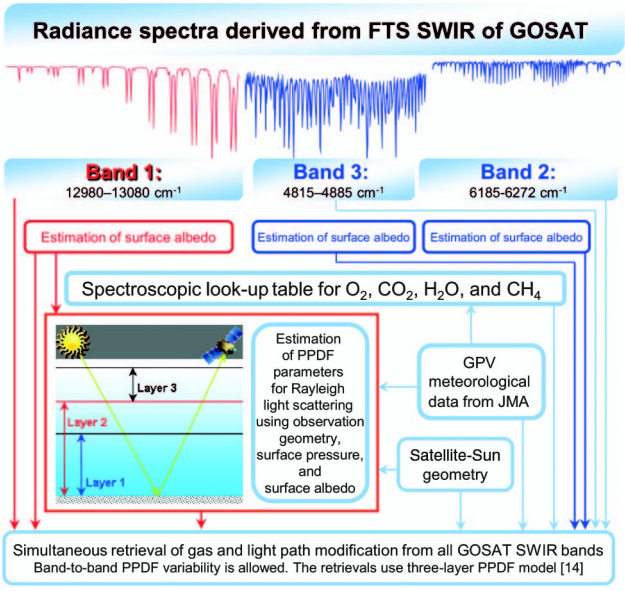

Fig. 1. Simplified flow chart showing the basic steps for the PPDF-S GOSAT data processing. Two overlapping layers from the surface to the variable retrieved altitudes (layers 1 and 2) allow for light path modification. The optical path within layer 3 (from the upper boundary of layer 2 to the top of the atmosphere) is not modified [14]. PPDF parameters for Rayleigh light scattering are pre-estimated in the oxygen A-band (0.76 μm) for layer 2. Aerosol/cloud PPDF parameters are retrieved simultaneously with gas amounts from all three GOSAT TANSO-FTS short-wavelength infrared (SWIR) bands for layer 1. The retrievals use a three-layer PPDF model [14] to account for light path modifications and up to 22 atmospheric layers to account for vertical distribution of gas absorption (meteorological parameters and gas profiles). Temperature and pressure grid point values were provided by Japan Meteorological Agency (JMA).

within the oxygen (O_2) A-band]. To incorporate variability in Rayleigh light scattering to the retrieval process, we use the three-dimensional PPDF [14]. This model permits an arbitrary number of gas layers and assumes three atmospheric layers within which the photon trajectories can be modified. The highest of the overlapping layers serves to describe light path modification by Rayleigh light scattering. The effective transmittance in this model has the following expression:

$$\tilde{T}_{\text{eff}} = \alpha_R \tilde{T}_3 + (1-\alpha_R)\tilde{T}_R \cdot \tilde{T}_a \cdot \tilde{T}_3, \quad (7)$$

$$T_3 = \exp[-A_G \cdot \tau_3], \quad (8)$$

$$\tilde{T}_R = \exp[-A_G \cdot (1+\delta_R) \cdot \tau_R], \quad (9)$$

$$\tilde{T}_a = (1-\alpha_a)\exp[-A_G \tau_a \delta_a] + \alpha_a \exp[+A_G \tau_a], \quad (10)$$

$$\delta_a = \rho_a \cdot \exp\{-\gamma_a \cdot \tau_a\}, \quad (11)$$

$$\delta_R = \rho_R \cdot \exp\{-\gamma_R \cdot \tau_R\}. \quad (12)$$

$\tau_a = \int_0^{h_a} k(h)\mathrm{d}h$, $\tau_R = \int_0^{h_R} k(h)\mathrm{d}h$, and $\tau_3 = \int_{h_R}^{h_A} k(h)\mathrm{d}h$ are the gaseous optical depth of the layers. In Eqs. (7)–(12), α, ρ, γ, and h are PPDF parameters, and subscripts R and a refer to upper and lower overlapping layers with the optical path perturbed by Rayleigh light scattering and combined Rayleigh and aerosol light scattering, respectively. PPDF parameters can be interpreted as follows [14]: α represents the relative layer reflectivity, i.e., the ratio of photons scattered by the layer to the total number of photons coming into the view of the detector; ρ is the scaled first moment of the PPDF within the layers describing multiple reflection of light within the layers; γ is an adjustment parameter used to account for the second and higher moments of the PPDF; and h_R and h_a are altitudes of layers with perturbed optical path by Rayleigh light scattering and aerosol light scattering, respectively.

For each satellite single sounding, PPDF parameters for atmospheric Rayleigh scattering were predefined using the actual observation geometry (i.e., solar and satellite zenith angles as well as relative azimuth angle), surface pressure and elevation, and surface albedo (for observations over land) or the Cox–Munk reflection model [29] with wind speed data from the Japan Meteorological Agency (JMA) (for observations over sea). With this information, we synthesize radiance spectra over a narrow subrange of the O_2 A-band (12,999 to 13,002 cm^{-1}) simulating radiative transfer in a Rayleigh-scattering atmosphere. These spectra were then converted to PPDF parameters using Eqs. (1)–(3) with the synthesized nonconvoluted radiance ($\boldsymbol{R}^*$). The forward model [$\boldsymbol{R}'(\boldsymbol{x})$] was based on Eqs. (4)–(12) under the assumption that the aerosol/cloud PPDF parameters in Eq. (5) are zero ($\alpha_a = \rho_a = 0$). Under predefined PPDF parameters for Rayleigh light scattering, we simultaneously retrieve aerosol/cloud PPDF parameters (α_a, ρ_a, h_a, γ_a) and CO_2 concentration vertical profiles $x_{\text{CO2}}(h)$ from the radiance in three bands and convert retrieved $\hat{x}_{\text{CO2}}(h)$ to the target quantity, the column-averaged dry air mole fractions of CO_2 (X_{CO2}),

$$\hat{X}_{\text{CO2}} = \frac{1}{\int_0^{h_A} N_{\text{dry}}(h)\mathrm{d}h} \int_0^{h_A} N_{\text{dry}} \hat{x}_{\text{CO2}}(h)\mathrm{d}h, \quad (13)$$

at a given pressure increment using the dry air number concentration $N_{\text{dry}}(h)$.

B. Retrieval Setup

For each satellite single scan, the state vector of simultaneously retrieved parameters x in Eq. (1) included the following:

- Vertical profiles of CO_2 volume mixing ratio equidistantly distributed on a pressure scale from the top of atmosphere to the surface (maximum 22 layers at surface pressure >1000 hPa).
- Four PPDF parameters, α_a, ρ_a, h_a, and γ_a, in each spectral band.
- A correction factor to scale the *a priori* water vapor profile.
- Three polynomial coefficients in Eq. (4) for each spectral band.
- A stretch factor to allow for possible distortion in the wavenumber grid for each spectral band.

Retrieval of PPDF parameter α_a was constrained within a physically allowable range $0 < \alpha_a \le 1$ by changing variables $\alpha_a = \exp\{-x_\alpha^2\}$ and retrieving the parameter x_α. We also constrain variability in ρ_a ($0 < \rho_a \le 1$) and γ_a ($2 < \gamma_a \le 3$) by retrieving x_ρ ($\rho_a = \exp\{-x_\rho^2\}$) and x_γ ($\gamma_a = 2 + \exp\{-x_\gamma^2\}$), respectively. The initial guesses for PPDF parameters α_a, ρ_a, and γ_a were 0.0001, 0.0001, and 2, respectively. Prior variance for PPDF parameter ρ_a was assumed to be 50% smaller for the observations over bight surface (gain M observation mode) than those for gain H observation mode [3,23]. We consider that the parameter α_a is inversely proportional to the surface albedo Γ. This follows from the proportionality of the "total number of photons coming into the view of the detector" (the denominator in α definition) to surface albedo. By this reason the initial guess 0.0001 in the gas absorption bands was applied to $\alpha_a^i = (\Gamma_1/\Gamma_i)\alpha_a^1$, where subscript $i = 1, 2, 3$ indicates the band number (0.76, 1.6, and 2.0 μm band). The surface albedo within each band was estimated as an average value from those estimated at the individual gas window channels (details are given elsewhere [13]). The initial guess of the altitude of aerosol layer h_a was 5 km. Both the initial guess and the prior of CO_2 dry-volume mixing ratio were an altitude-independent profile of 385 ppm. The prior covariance matrix has the following expression:

$$C_a^{ii'} = \sqrt{C_a^{ii} \cdot C_a^{ii'}} \cdot \exp\left\{-\zeta \cdot \left|\ln\left(\frac{p_i}{p_{i'}}\right)\right|\right\}. \quad (14)$$

This implies altitude-independent variance C_a^{ii} at each pressure level and an exponential dependence for the off-diagonal elements of the covariance matrix on the distance between the pressure levels [30] (in units of ln p). We set up the scaling factor ζ to 5 and *a priori* CO_2 variance C_a^{ii} so that the *a priori* CO_2 standard deviation X_{CO2} was 6 ppm. Surface pressure and temperature profiles were predefined using data from the JMA.

We apply a postprocessing quality assessment to accept only those retrievals for which $\chi^2 < 5$ [Eq. (2)], signal-to-noise ratio SNR ≥ 75 for each spectral band, degrees of freedom for the signal DFS > 1 [30] (to ensure the low impact of *a priori* assumptions on *a posteriori* X_{CO2} estimations), and the *a posteriori* error estimate ≤1.25 ppm. We also filter out the estimated X_{CO2} with large optical path modification in the CO_2 1.6 μm band ($\hat{\alpha}_a > 0.1$, $\hat{\rho}_a > 0.1$) where the gas retrievals could be questionable or impractical (up to 10% contribution from light path modification). The retrieved values of ρ_a were limited to 0.01 over oceans or lakes. We include this for physical reasons: the fraction of photons that contribute to the measured signal after interacting with both dark sea surface and aerosols or subvisible clouds should be very low [31].

3. FTS Data

A. GOSAT

GOSAT has flown in a Sun-synchronous orbit since 23 January 2009 with an equator crossing time of about 13:00 local time, completes an orbit in about 100 min, and operates on a global basis with a 3 day repeat cycle at an altitude of approximately 666 km.

GOSAT is equipped with two instruments, the thermal and near-infrared sensor for carbon observation–Fourier transform spectrometer (TANSO-FTS) and the TANSO cloud and aerosol imager (TANSO-CAI). Both instruments have been described in detail in [3]. While TANSO-CAI is an ancillary imager mainly used to identify the clear sky atmospheric conditions [21,32], TANSO-FTS is the key instrument for observing the gas composition. The raw interferograms (Level 1A; L1A data) directly measured by TANSO-FTS are then transformed to radiance spectra (Level 1B; L1B data). In this study we utilize TANSO-FTS radiance spectra in three narrow bands in the short-wavelength infrared (SWIR) region (0.76, 1.6, and 2.0 μm as the center; also referred to as TANSO-FTS bands 1, 2, and 3, respectively). These spectra are measured at a high spectral resolution (interval) of about 0.2 cm^{-1}. The TANSO-FTS collects data within an instantaneous, circular field of view with a 15.8 mrad diameter that corresponds to approximately 10.5 km diameter footprints at the Earth's surface for nadir observations.

In this study, we analyze Level 2 (L2) data (X_{CO2}) derived from 14 months of GOSAT operation from June 2009 to July 2010. In this period, a recently updated version of L1B (from V.141.141) data derived from the TANSO-FTS has been applied to L2 data processing. We also consider only those "clear sky" GOSAT soundings that have passed the TANSO-CAI cloud flag test [21].

B. TCCON

The ground-based high-resolution FTS observations from TCCON [24] were established in 2004 to provide a transfer standard between satellite observations and ground-based *in situ* measurements. TCCON has become a reliable reference source of greenhouse gas measurements due to its direct solar-viewing geometry that practically eliminates the impact of atmospheric light scattering on the measurements. The uncertainties in a column-averaged CO_2 amount from the ground-based FTS measurement network were estimated to be mostly within 1 ppm by comparing the TCCON retrievals with aircraft measurements [33–35].

Twelve TCCON sites have been selected for the GOSAT coincident observations, namely, 9 sites in the Northern Hemisphere: Bialystok, Poland (53.2°N, 23.1°E); Bremen, Germany (53.1°N, 8.85°E); Garmisch, Germany (47.5°N, 11.1°E); Izaña, Spain (28.3°N, 16.48°W); Lamont, USA (36.6°N, 97.5°W); Orleans, France (48.0°N, 2.11°E); Park Falls, USA (45.9°N, 90.3°W); Sodankyla, Finland (67.4°N, 26.6°E); and Tsukuba, Japan (36.0°N, 140.2°E); and three sites from the Southern Hemisphere: Darwin, Australia (12.4°S, 130.9°E); Lauder, New Zealand (45.0°S, 169.7°E); and Wollongong, Australia (34.4°S, 150.9°E). Fig. 2 illustrates the global locations of these TCCON stations (yellow stars).

The TCCON–GOSAT coincidence criteria for validating the satellite-based retrievals included GOSAT single scan data within a 5° radius latitude/longitude circle centered at each TCCON station. Retrievals from observations over both land and ocean/lakes were considered within this circle. Over the Izaña site, we examine GOSAT observations collected from a larger sampling domain (within 15° latitude × 45° longitude grid box), which partly covers the Sahara desert and North Atlantic Ocean, as shown in Fig. 3. In these regions mechanisms of light path modifications diverged considerably due to different surface reflective properties. The ground-based TCCON data (GGG2009 release, last updated 2011) treated in this study are mean values measured within ±1 h of the GOSAT overpass time (at around 13:00 local time).

4. CO_2 Retrievals from GOSAT Observations

In this section we compare X_{CO2} PPDF-S retrievals from GOSAT to TCCON ground-based FTS measurements. For reference, two other algorithms [National Institute for Environmental Studies (NIES) PPDF-D and NIES V02.00] previously developed for

Fig. 2. Global locations of operational TCCON sites (yellow stars) whose ground-based FTS measurements were used in validation of GOSAT X_{CO2} retrievals.

GOSAT data processing have been included in this comparison.

A. Observations over Izaña Site

The Izaña site has a unique location for providing validation of satellite-based measurements both over dark (ocean) and bright (western part of Sahara desert) surfaces. High-altitude cirrus or sand storm activities over these surfaces could produce very large light path modification [28]. In this study we have chosen a sampling domain collecting GOSAT data within a 15° latitude × 45° longitude grid box (yellow rectangle in Fig. 3). Since the sampling domain is large, atmospheric transport model calculations have been invoked to control the natural variability in X_{CO2} within this sampling grid box when comparing GOSAT observations with TCCON measurements. The NIES global atmospheric tracer

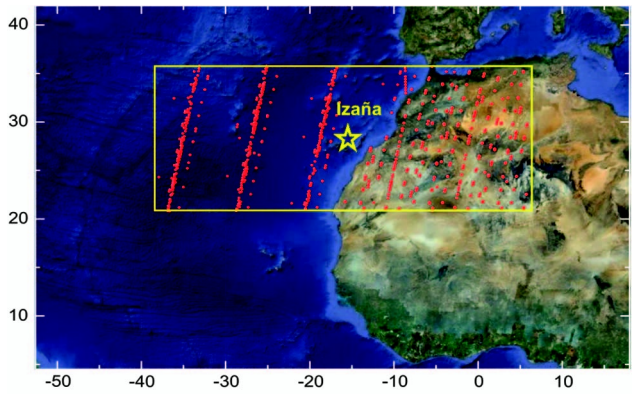

Fig. 3. GOSAT sampling domain (15° latitude × 45° longitude grid box, yellow rectangle) around Izaña TCCON site (yellow star). Red symbols indicate the location of GOSAT single soundings available for data processing from June 2009 to July 2010. 92% of GOSAT soundings over land (northern Africa) were derived under GOSAT gain M mode, indicating bright Saharan desert surfaces. Only sun glint areas were available to measure over the ocean due to the sufficient reflected signals, so strips are seen in the map.

transport model (present version NIES 08.1i) used in this study has been described in [36] and outlined in [18]. We will refer to this model as NIES-TM.

Figure 4 shows seasonal variability in X_{CO2} from GOSAT (gray crosses and open blue symbols), from TCCON (solid red symbols), and from the NIES-TM calculations (green and dark yellow symbols). Gray crosses indicate original scan-to-scan retrievals and open blue symbols correspond to weekly mean X_{CO2} with bars representing standard deviation. GOSAT data at the bottom of Fig. 4 display retrievals with the PPDF-S algorithm. GOSAT X_{CO2} data in top and middle panels were retrieved with PPDF-D algorithm. We present X_{CO2} data derived from GOSAT separately over land (left-hand panels) and sea (right-hand panels). To increase the measurement dynamic range, the GOSAT TANSO-FTS collects data over land either in "high gain" (Gain H) state (over most surfaces) or in "middle gain" (Gain M) mode (over bright surfaces). We found that 92% of GOSAT land observations within the rectangle of Fig. 3 were derived under the TANSO-FTS instrument middle gain (Gain M) state, which is to say that most of these observations were over bright desert surfaces. The overwhelming majority of over-sea GOSAT observations were under high gain (Gain H) mode. Using the NIES-TM simulation, we found that the standard deviation of daily mean X_{CO2} data within ±1 h of GOSAT overpass time within this sampling domain is <1.5 ppm. As a pictorial example, green and dark yellow symbols in Fig. 4 display daily mean seasonal trends of modeled X_{CO2} at +20° and −20° longitude shift from the Izaña site, respectively.

As is seen from the bottom panels of Fig. 4, PPDF-S retrievals reproduce the temporal patterns in X_{CO2} observed in the TCCON measurements and simulated by NIES-TM well. A clear and pronounced seasonal cycle of X_{CO2} can be seen, with minima in late summer and maxima in spring. The seasonal gap of GOSAT data over the ocean from September 2009 to March 2010 (right-hand panels of Fig. 4) stems from

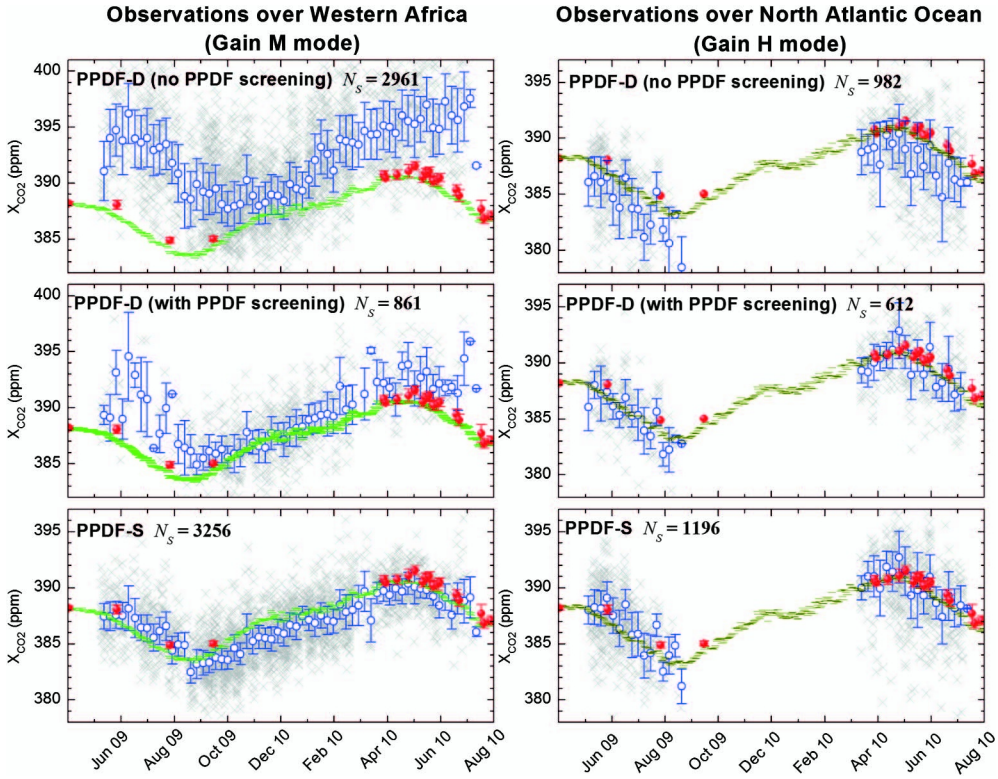

Fig. 4. Time series that correspond to GOSAT single scan X_{CO2} (gray crosses), GOSAT weekly mean X_{CO2} data (open blue symbols with bars representing standard deviation), single scan ground-based FTS measurement (solid red symbols), and daily mean X_{CO2} atmospheric model (green and dark yellow symbols) over the Izaña site. GOSAT data were collected within a 15° latitude × 45° longitude grid box centered at Izaña (Fig. 3) and presented separately for observations over land (western Africa, left-hand panel) and sea (North Atlantic Ocean, right-hand panel). Top to bottom panels correspond to different GOSAT X_{CO2} retrieval algorithms (indicated in the legends of the panels). Green and dark yellow symbols correspond to modeled X_{CO2} at −20° and +20° longitude shift from Izaña site, respectively. N_S indicates the number of GOSAT soundings accessible to be processed.

the absence of GOSAT sun glint observations due to the low solar elevation angle in this period. It should be noted that TCCON X_{CO2} measurements (solid red symbols) ignored contribution of CO_2 in boundary layer because the site is located at the mountain Izaña (2370 m above sea level). According to our estimation based on the modeled CO_2 profiles near the Izaña site, neglect of CO_2 contribution below the level of site location leads to sub-ppm seasonally variable X_{CO2} bias. In particular, this bias was negative from April to June (up to 0.7 ppm) and positive in August and September (up to 0.35 ppm).

Figure 4 demonstrates that simultaneous gas and light path retrievals with the PPDF-S algorithm have a significant advantage over gas retrievals from the PPDF-D algorithm. As noted earlier, the PPDF-D algorithm retrieves gas amounts under conditions where the optical path modification can be assumed to be negligible (Section 2.A), which is achieved by PPDF prescreening (Section 2.B). To demonstrate that the improvement of gas retrievals is provided by accurate light path correction, we have selected only those GOSAT soundings for PPDF-D data processing that are coincident with the selected PPDF-S data set (after postprocessing filters, Section 2.B). The upper panels in Fig. 4 display PPDF DOAS-based retrieval results before applying the PPDF-D screening in the O_2 A-band (see Section 2.A). The scan numbers, N_S, accessible to the processing (see legend of each panel) is slightly lower here (2961 over land; 982 over ocean) than those from PPDF-S (3256 over land; 1196 over ocean) because a number of scans were rejected by other PPDF-D filters, such as by the pure spectral fit [in Eq. (2)]. PPDF DOAS-based retrievals showed substantial overestimation of gas amounts over bright surfaces (top left-hand panel in Fig. 4) [11,28]. These positive biases resulted from multiple reflections of light between a bright surface and an aerosol layer or high-altitude subvisible cloud [28], which lengthened the imperturbable light path [Eq. (12)]. In contrast, aerosol and cloud light scattering over dark surfaces, such as the ocean, resulted in underestimated gas retrievals (top right-hand panel of Fig. 4) [12,28]. This is a consequence of shortening the light path when the fraction of photons that reach the detector after being scattered by atmospheric aerosol and then reflected by the dark surface should be rather small [28]. PPDF selection ($\alpha < 0.04$ and $\rho < 0.04$) improves the DOAS-based retrievals (middle panels of Fig. 4), but the number of scans available for processing is substantially decreased, especially over the Sahara desert. It is also worth noting that there appears to be a positive bias even in the remaining scans in

the summer seasons. As noted above, PPDF-D and PPDF-S algorithms used similar sets of GOSAT scans. Thus, accurate light path correction is primarily responsible for the improvements of gas retrievals with PPDF-S algorithm (bottom panels in Fig. 4).

Figure 5 displays the seasonal variability in PPDF parameters α (upper panels) and ρ (middle panels) retrieved simultaneously with gas concentration according to PPDF-S (Fig. 4) over western Africa (left-hand panel) and over Atlantic Ocean (right-hand panel). As expected, values of the PPDF parameter α are much lower than ρ over bright Sahara desert surfaces representing the trend of increasing path length due to multiple reflections of photons between aerosol/cirrus and bright surface. We found pronounced enhancement of ρ from April to August (middle left-hand panel of Fig. 5) that is probably associated with summer dust storm activity in the Sahara desert. Indeed, the DOAS-based X_{CO2} retrievals over the Sahara desert were the most biased in this period (top left-hand panel in Fig. 4). Overall this agrees with seasonal variability in the aerosol optical depth (AOD) (bottom panels in Fig. 5) calculated from an offline three-dimensional aerosol transport model, the Spectral Radiation-Transport Model for Aerosol Species (SPRINTARS version 3.84) [37]. The AOD data presented in Fig. 5 correspond to those GOSAT observation scans that were available for processing with the PPDF-S method; that is, the GOSAT scenes with very large aerosol loadings were rejected by the CAI test or PPDF-S filters. The Pearson correlation coefficient between parameter ρ and AOD was 0.57 over the Sahara desert. The total AOD included both fine and coarse modes of aerosol particles. For the coarse mode of large particles the correlation coefficient was slightly larger. The correlation coefficient between α parameters, which is more representative for describing light path modification over dark ocean surfaces, was lower but positive (0.26). It should be noted that the optical path change need not be tightly correlated with the AOD because the light path depends not only on the aerosol amount but also on the surface reflective properties and on the vertical location of the aerosol layer.

B. Pairwise GOSAT–TCCON Comparison

In this section, we compare GOSAT X_{CO2} retrievals from the PPDF-S algorithm with ground-based TCCON measurements of CO_2 column-averaged abundance collecting GOSAT–TCCON coincident observations (Section 3.B) over 11 TCCON sites (Fig. 2).

The bottom panels of Fig. 6 summarize the pairwise statistical comparison between GOSAT

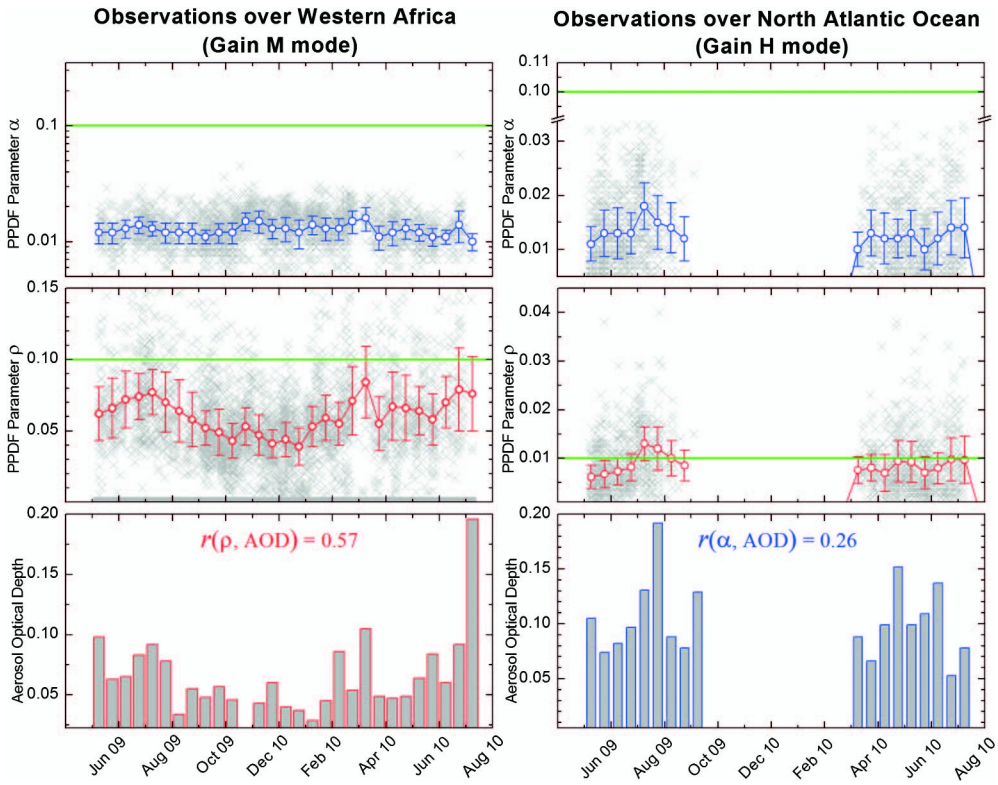

Fig. 5. Time series of PPDF parameters α (top panels) and ρ(middle panels) retrieved with PPDF-S algorithm from single GOSAT scans (gray crosses) and weekly mean PPDF data (open circles with bars representing standard deviation). GOSAT data were collected within 15° latitude × 45° longitude grid box centered at Izaña site (Fig. 3) and presented separately for observations over land (western Africa, left-hand panel) and over sea (North Atlantic Ocean, right-hand panel). Green lines indicate the threshold of PPDF parameters beyond which the retrievals were rejected according to postprocessing filter (Section 2.B). Histograms in the bottom panels represent seasonal variability in the total AOD (averaged over 15 days at 1.6 μm) from a global three-dimensional aerosol transport-radiation model.

PPDF-S and TCCON X_{CO2} data within the coincidence criterion. In Fig. 6 we present GOSAT–TCCON X_{CO2} correlation diagrams separately over the Lamont site (left-hand panels), over the other seven Northern Hemisphere sites (middle panels) (Izaña is excluded here), and over three Southern Hemisphere sites (right-hand panels). The results over the Lamont site are shown separately in Fig. 6 as the GOSAT observations over this site had the largest sample size due to multiple orbit overpasses within the coincidence criteria and comparatively clear skies. The coincident GOSAT–TCCON observation numbers (N_C) as well as statistical characteristics of the GOSAT–TCCON X_{CO2} relationship for each set of stations are in the legend of each panel. We present the following statistical characteristics: bias (*Bias*); standard deviation (σ); Pearson's correlation coefficient (r), and coefficient of determination (goodness of fit) (R^2) between GOSAT and TCCON X_{CO2}. To allow for uncertainties in both data sources when comparing these data, we use a weighted least-squares fit to minimize the square of the perpendicular distances between GOSAT and TCCON X_{CO2} data [38]. Accordingly, the statistical characteristics can be calculated using standard weighed least squares (equations can be found in [18]) with covariance matrix

$$C_{ii'} = (\sigma_{Gi}^2 + a^2\sigma_{Fi}^2)\delta_{ii'}, \tag{15}$$

where $\delta_{ii'}$ is the Kronecker delta indicating zero off-diagonal elements of the covariance matrix, a is a slope for the slope-intercept form of the linear regression, and σ_{Gi} and σ_{Fi} are the standard deviations of the individual GOSAT and TCCON sounding, respectively. The best fits obtained are plotted in Fig. 6 by red lines; the dashed red lines and the green lines represent the best fit $\pm\sigma$ and the one-to-one correspondence, respectively.

The slope a, which is known to be an important measure when characterizing the bias correction, is perfect (1.00) when comparing GOSAT and TCCON X_{CO2} data over Lamont (bottom left-hand panel in Fig. 6) and equal to 0.96 over all other TCCON sites in the

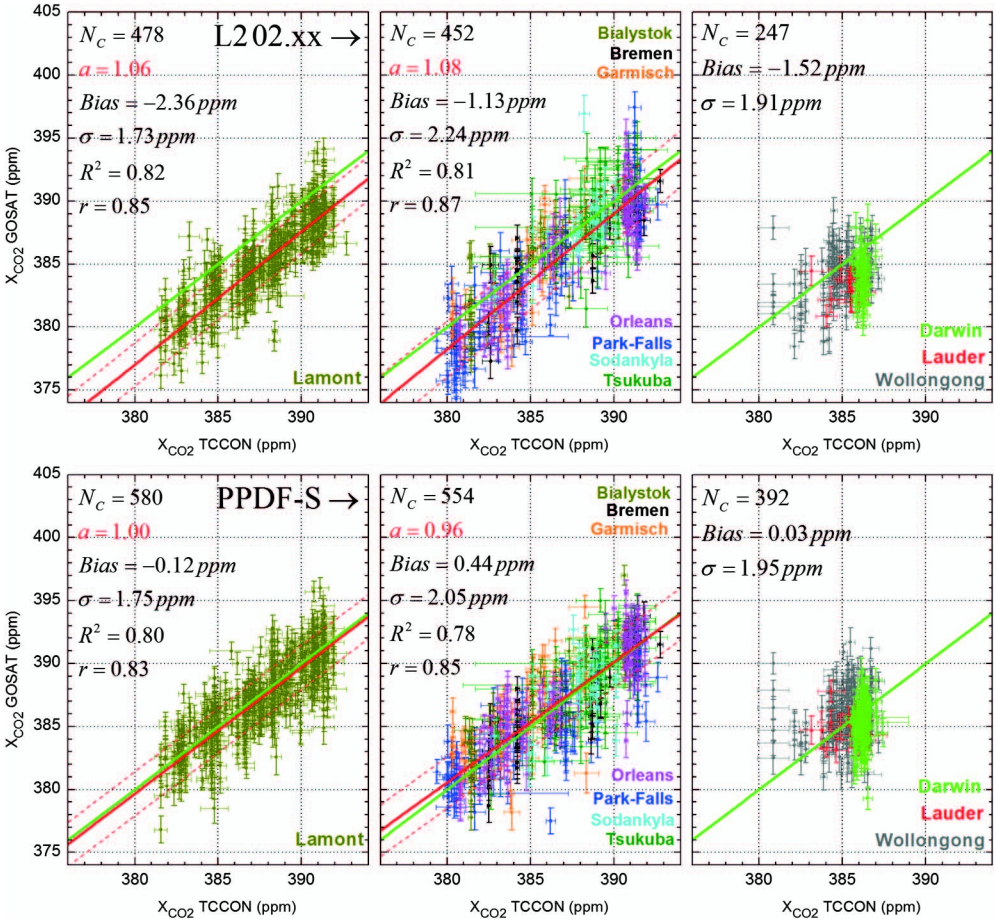

Fig. 6. Correlation diagrams between GOSAT and ground-based TCCON measurements of X_{CO2} for two GOSAT retrieval algorithms, PPDF-S (bottom panels) and NIES L2 02.xx (top panels), and for three sets of TCCON sites, over Lamont (left-hand panels), over the other seven Northern Hemisphere sites (middle panels), and over three Southern Hemisphere sites (right-hand panels). The GOSAT single scans were selected during 14 months from June 2009 within a 5° radius latitude/longitude circle centered over each TCCON station. The analyzed ground-based FTS data were mean values measured within ±1 h of the GOSAT overpass time. Red lines correspond to the best fits, and the green line represents one-to-one correspondence. The number of coincident soundings and characteristics of statistical relationships between ground-based FTS and GOSAT X_{CO2} for each set of TCCON stations is listed in the legend of each panel.

Northern Hemisphere (bottom middle panel in Fig. 6). We do not present slope, correlation coefficients, and coefficients of determination for the three operational Southern Hemisphere stations in the right-hand panels of Fig. 6 because these characteristics are not representative here due to the low variability in X_{CO2} over the Southern Hemisphere sites. For the coincident measurements over all 11 TCCON stations, both in the Northern and Southern Hemisphere, GOSAT and TCCON data of CO_2 column-averaged abundance showed a slope of 0.96 for the slope-intercept form of the linear regression, a correlation coefficient of 0.83, a standard deviation of 1.90 ppm, and a very small negative bias of 0.08 ppm (not shown in Fig. 6).

For reference, the upper panels of Fig. 6 display the GOSAT–TCCON X_{CO2} comparison according to SWIR L2 V02.00 "full physics" (FP) algorithm that operationally processes the GOSAT data at NIES. The basic performances of NIES FP algorithm were described in [21] (V01.00) and its important improvements were outlined in [23] (V02.00). There are many common features in NIES 02.xx and PPSD-S retrieval setup. For example, they both use similar solar irradiance spectra and gas data sets, process GOSAT data from all three GOSAT SWIR bands, initially retrieve the CO_2 profile based on the maximum *a posteriori* rule [Eq. (1)], retrieve a stretch factor to allow for distortion in the wavenumber grid and adjust water vapor amounts, etc. [23]. As with any other FP approach [15,17,19,20–22], this algorithm is distinct from PPDF-S via its radiative transfer modeling. While PPDF-S deals with statistical properties of the optical path through the atmosphere, V02.00 accounts for atmospheric light scattering by considering the variability in a limited number of aerosol components. These components are incorporated in the retrieval process using the numerical solution of the radiative transfer equation at each spectral line. NIES 02.00 uses two aerosol components: fine and coarse modes of aerosol particles (SPRINTARS version 3.84) [37]. The vertical profiles of the aerosol number density for each component are included in the state vector and retrieved simultaneously with gas profiles. This algorithm also retrieves surface pressure in the O_2 A-band. Generally, the latter permits estimation of light path modification looking at the deviation between the retrieved surface pressure and its meteorological prior (e.g., [23]). However, this estimation could be biased due to a tight correlation between surface pressure and aerosol characteristics, which are retrieved simultaneously in the O_2 A-band. In addition, the light path detection based on the surface pressure retrievals could characterize only the integrated effect of the optical path modification. Therefore, there is always a risk that the GOSAT scans with a nonmodified retrieved surface pressure might be misinterpreted as clear-sky scenes when effects of optical path lengthening and shortening are compensatory [13]. This could frequently happen under a fortuitous combination of aerosol, cloud, and surface optical properties [20,23]. Finally, the light path modification in the O_2 A-band is not always appropriate for characterizing the light path in the target gas bands. The PPDF-S algorithm avoids these problems by retrieving both optical path lengthening and shortening in the gas absorption bands (Section 2).

Our recent study [23] has indicated that the NIES V02.00 algorithm provided one of the best slope, correlation and determination coefficients, standard deviation, and large sampling size when comparing GOSAT X_{CO2} retrievals from all FP algorithms with TCCON measurements. This comparison was performed with similar GOSAT–TCCON coincident criteria (within a 5° radius over 11 TCCON sites) during 22 months of GOSAT operation of from June 2009 to March 2011 using older versions of L1B GOSAT data. As evident from the legends of Fig. 6, PPDF-S retrievals showed similar GOSAT–TCCON X_{CO2} agreement as compared with those derived from V02.00 algorithm by most of these statistical characteristics providing larger sampling size over both the Northern Hemisphere (by >20%) and Southern Hemisphere (by >50%) sites and much lower global bias. Both systematic negative bias (−1.74 ppm over all TCCON sites) and comparatively large station-to-station bias from the V02.xx algorithm (upper panels of Fig. 6) were previously detected in [23]. This tendency remains for the data set used in this study: the station-to-station bias reaches 1.24 ppm (−0.12 to −1.13). PPDF-S retrievals provide a sub-ppm station-to-station bias of 0.6 ppm (−0.12 to +0.44 ppm).

5. Conclusions

In this study, we introduced an improved version of the PPDF method (PPDF-S) that accounts for atmospheric light scattering when processing space-based spectroscopic observations of greenhouse gases. This method provides simultaneous gas and optical path retrievals using high-resolution spectroscopic observations in three short-wave infrared bands at 0.76, 1.6, and 2.0 μm. This allows for satellite data processing under non-negligible light path modifications, which, due to light path correction, substantially increases the number of observations available for data processing with accurate gas retrievals. The radiative transfer model is based on three-dimensional PPDF, which assumes three atmospheric layers within which the photon trajectories can be modified, and permits retrieval on an arbitrary number of gas layers.

The PPDF-S method was applied to processing GOSAT observations during 14 months from June 2009 to July 2010. We focus on the comparison of the satellite-based retrievals of column-averaged CO_2 amounts with those provided by ground-based FTS measurements at 12 TCCON sites.

First, we analyzed GOSAT PPDF-S retrievals over the Izaña TCCON site collecting the GOSAT observations within a large sampling domain (15° latitude × 45° longitude grid box) that covers both dark (northern Atlantic Ocean) and bright

(western part of the Sahara desert) surfaces and, therefore, is representative of conditions where we expect light path shortening and lengthening due to high-altitude cirrus or coarse aerosol particles from Saharan dust. Using coincident GOSAT–TCCON observations, both from PPDF-S and DOAS-based retrievals, we have demonstrated considerable improvements in the gas retrievals and proved that this improvement is due to light path corrections.

Next, we have performed a statistical pairwise comparison between X_{CO2} GOSAT PPDF-S retrievals and TCCON ground-based measurements collecting GOSAT observations within a 5° radius latitude/longitude circle centered at each TCCON station. We found 1526 coincident GOSAT–TCCON single scans accessible for the comparison. Over all 11 TCCON stations, in both the Northern and Southern Hemisphere, the correlation diagrams showed a slope of 0.96 for the slope-intercept form of the linear regression, a correlation coefficient of 0.83, a standard deviation of 1.90 ppm, and a very small negative bias of 0.08 ppm. We found that PPDF-S retrievals are highly competitive with those derived from the V02.xx algorithm when comparing both algorithms with TCCON measurements. Both algorithms provide similar GOSAT–TCCON X_{CO2} correlation coefficients and standard deviation. At the same time, PPDF-S provided a larger sampling size over both Northern Hemisphere sites (by >20%) and Southern Hemisphere sites (by >50%) and lower sub-ppm interstation X_{CO2} bias.

GOSAT is a joint effort of the Japan Aerospace Exploration Agency (JAXA), the NIES, and the Ministry of the Environment (MOE), Japan. TCCON data were obtained from the TCCON Data Archive, operated by the California Institute of Technology from the website at http://tccon.ipac.caltech.edu/. The authors thank TCCON partners Paul Wennberg, David Griffith, Esko Kyrö, Pauli Heikkinen, and Vanessa Sherlock for their valuable contribution to TCCON measurements used in this study. U.S. funding for TCCON is provided by NASA's Terrestrial Ecology program (grant number NNX11AG01G), the Orbiting Carbon Observatory program, the Atmospheric CO_2 Observations from Space (ACOS) program, and the Department of Energy/Atmospheric Radiation Measurement (DOE/ARM) program. The Darwin TCCON site was built at Caltech with funding from the OCO project, and is operated by the University of Wollongong, with travel funds for maintenance and equipment costs funded by the OCO-2 project. We acknowledge funding to support Darwin and Wollongong from the Australian Research Council projects LE0668470, DP0879468, DP110103118, and LP0562346. Lauder TCCON measurements are funded by New Zealand Foundation of Research Science and Technology contracts C01X0204 and CO1X0406. We acknowledge financial support of the Białystok and Orléans TCCON sites from the Senate of Bremen and EU projects IMECC, GEOMON, and InGOS as well as maintenance and logistical work provided by AeroMeteo Service (Białystok) and the RAMCES team at LSCE (Gif-sur-Yvette, France) and additional operational funding from the NIES GOSAT project. The Garmisch TCCON team acknowledges funding by the EC-INGOS project. We also would like to thank the members of the NIES GOSAT and the NASA Atmospheric CO_2 Observations from Space (ACOS) projects for helpful comments and discussions.

References

1. T. Hamazaki, Y. Kaneko, A. Kuze, and K. Kondo, "Fourier transform spectrometer for Greenhouse Gases Observing Satellite (GOSAT)," Proc. SPIE **5659**, 73–80 (2005).
2. T. Yokota, Y. Yoshida, N. Eguchi, Y. Ota, T. Tanaka, H. Watanabe, and S. Maksyutov, "Global concentrations of CO_2 and CH_4 retrieved from GOSAT: first preliminary results," Sci. Online Lett. Atmos. **5**, 160–163 (2009).
3. A. Kuze, H. Suto, M. Nakajima, and T. Hamazaki, "Thermal and near infrared sensor for carbon observation Fourier-transform spectrometer on the Greenhouse Gases Observing Satellite for greenhouse gases monitoring," Appl. Opt. **48**, 6716–6733 (2009).
4. P. J. Rayner and D. M. O'Brien, "The utility of remotely sensed CO_2 concentration data in surface source inversions," Geophys. Res. Lett. **28**, 175–178 (2001).
5. C. E. Miller, D. Crisp, P. L. DeCola, S. C. Olsen, J. T. Randerson, A. M. Michalak, A. Alkhaled, P. Rayner, D. J. Jacob, P. Suntharalingam, D. B. A. Jones, A. S. Denning, M. E. Nicholls, S. C. Doney, S. Pawson, H. Boesch, B. J. Connor, I. Y. Fung, D. O'Brien, R. J. Salawitch, S. P. Sander, B. Sen, P. Tans, G. C. Toon, P. O. Wennberg, S. C. Wofsy, Y. L. Yung, and R. M. Law, "Precision requirements for space-based X_{CO2} data," J. Geophys. Res. **112**, D10314 (2007).
6. F. Chevallier, S. Maksyutov, P. Bousquet, F.-M. Bréon, R. Saito, Y. Yoshida, and T. Yokota, "On the accuracy of the CO_2 surface fluxes to be estimated from the GOSAT observations," Geophys. Res. Lett. **36**, L19807 (2009).
7. N. Kadygrov, S. Maksyutov, N. Eguchi, T. Aoki, T. Nakazawa, T. Yokota, and G. Inoue, "Role of simulated GOSAT total column CO_2 observations in surface CO_2 flux uncertainty reduction," J. Geophys. Res. **114**, D21208 (2009).
8. D. M. O'Brien and P. J. Rayner, "Global observations of the carbon budget, 2, CO_2 column from differential absorption of reflected sunlight in the 1.61 μm band of CO_2," J. Geophys. Res. **107**, 4354 (2002).
9. E. Dufour and F.-M. Bréon, "Spaceborne estimate of atmospheric CO_2 column by use of the differential absorption method: error analysis," Appl. Opt. **42**, 3595–3609 (2003).
10. J. Mao and S. R. Kawa, "Sensitivity studies for space-based measurement of atmospheric total column carbon dioxide by reflected sunlight," Appl. Opt. **43**, 914–927 (2004).
11. S. Houweling, W. Hartmann, I. Aben, H. Schrijver, J. Skidmore, G.-J. Roelofs, and F.-M. Breon, "Evidence of systematic errors in SCIAMACHY-observed CO_2 due to aerosols," Atmos. Chem. Phys. **5**, 3003–3013 (2005).
12. I. Aben, O. Hasekamp, and W. Hartmann, "Uncertainties in the space-based measurements of CO_2 columns due to scattering in the Earth's atmosphere," J. Quant. Spectrosc. Radiat. Transfer **104**, 450–459 (2007).
13. S. Oshchepkov, A. Bril, and T. Yokota, "PPDF-based method to account for atmospheric light scattering in observations of carbon dioxide from space," J. Geophys. Res. **113**, D23210 (2008).
14. S. Oshchepkov, A. Bril, and T. Yokota, "An improved photon path length probability density function-based radiative transfer model for space-based observation of greenhouse gases," J. Geophys. Res. **114**, D19207 (2009).
15. M. Reuter, M. Buchwitz, O. Schneising, J. Heymann, H. Bovensmann, and J. P. Burrows, "A method for improved SCIAMACHY CO_2 retrieval in the presence of optically thin clouds," Atmos. Meas. Tech. **3**, 209–232 (2010).

16. A. Bril, S. Oshchepkov, T. Yokota, and G. Inoue, "Parameterization of aerosol and cirrus cloud effects on reflected sunlight spectra measured from space: application of the equivalence theorem," Appl. Opt. **46**, 2460–2470 (2007).
17. B. J. Connor, H. Boesch, G. Toon, B. Sen, C. Miller, and D. Crisp, "Orbiting Carbon Observatory: inverse method and prospective error analysis," J. Geophys. Res. **113**, D05305 (2008).
18. S. Oshchepkov, A. Bril, T. Yokota, I. Morino, Y. Yoshida, T. Matsunaga, D. Belikov, D. Wunch, P. Wennberg, G. Toon, C. O'Dell, A. Butz, S. Guerlet, A. Cogan, H. Boesch, N. Eguchi, N. Deutscher, D. Griffith, R. Macatangay, J. Notholt, R. Sussmann, M. Rettinger, V. Sherlock, J. Robinson, E. Kyrö, P. Heikkinen, D. G. Feist, T. Nagahama, N. Kadygrov, S. Maksyutov, O. Uchino, and H. Watanabe, "Effects of atmospheric light scattering on spectroscopic observations of greenhouse gases from space. Part 1: validation of PPDF-based CO_2 retrievals from GOSAT," J. Geophys. Res. **117**, D12305 (2012).
19. A. Butz, O. P. Hasekamp, C. Frankenberg, and I. Aben, "Retrievals of atmospheric CO_2 from simulated space-borne measurements of backscatter near-infrared sunlight: accounting for aerosol effects," Appl. Opt. **48**, 3322–3336 (2009).
20. C. W. O'Dell, B. Connor, H. Boesch, D. O'Brien, C. Frankenberg, R. Castano, M. Christi, D. Crisp, A. Eldering, B. Fisher, M. Gunson, J. McDuffie, C. E. Miller, V. Natraj, F. Oyafuso, I. Polonsky, M. Smyth, T. Taylor, G. C. Toon, P. O. Wennberg, and D. Wunch, "The ACOS CO_2 retrieval algorithm—part 1: description and validation against synthetic observations," Atmos. Meas. Tech. **5**, 99–121 (2012).
21. Y. Yoshida, Y. Ota, N. Eguchi, N. Kikuchi, K. Nobuta, H. Tran, I. Morino, and T. Yokota, "Retrieval algorithm for CO_2 and CH_4 column abundances from short-wavelength infrared spectral observations by the Greenhouse Gases Observing Satellite," Atmos. Meas. Tech. **4**, 717–734 (2011).
22. A. J. Cogan, H. Boesch, R. J. Parker, L. Feng, P. I. Palmer, J.-F. L. Blavier, N. M. Deutscher, R. Macatangay, J. Notholt, C. Roehl, T. Warneke, and D. Wunch, "Atmospheric carbon dioxide retrieved from the Greenhouse Gases Observing SATellite: comparison with ground-based TCCON observations and GEOS-Chem model calculations," J. Geophys. Res. **117**, D21301 (2012).
23. S. Oshchepkov, A. Bril, T. Yokota, P. Wennberg, N. M. Deutscher, D. Wunch, G. C. Toon, Y. Yoshida, C. W. O'Dell, D. Crisp, C. E. Miller, C. Frankenberg, A. Butz, I. Aben, S. Guerlet, O. Hasekamp, H. Boesch, A. Cogan, R. Parker, D. Griffith, R. Macatangay, J. Notholt, R. Sussmann, M. Rettinger, V. Sherlock, J. Robinson, E. Kyrö, P. Heikkinen, D. G. Feist, I. Morino, N. Kadygrov, D. Belikov, S. Maksyutov, T. Matsunaga, O. Uchino, and H. Watanabe, "Effects of atmospheric light scattering on spectroscopic observations of greenhouse gases from space. Part 2: algorithm intercomparison in the GOSAT data processing for CO_2 retrievals over TCCON sites," J. Geophys. Res. (to be published).
24. D. Wunch, G. C. Toon, J.-F. L. Blavier, R. A. Washenfelder, J. Notholt, B. J. Connor, D. W. T. Griffith, V. Sherlock, and P. O. Wennberg, "The Total Carbon Column Observing Network," Phil. Trans. R. Soc. A **369**, 2087–2112 (2011).
25. R. Bennartz and R. Preusker, "Representation of the photon path-length distribution in a cloudy atmosphere using finite elements," J. Quant. Spectrosc. Radiat. Transfer **98**, 202–219 (2006).
26. M. Buchwitz, V. Rozanov, and J. P. Burrows, "A near-infrared optimized DOAS method for the fast global retrieval of atmospheric CH_4, CO, CO_2, H_2O, and N_2O total column amounts from SCIAMACHY Envisat-1 nadir radiances," J. Geophys. Res. **105**, 15231–15245 (2000).
27. C. Frankenberg, U. Platt, and T. Wagner, "Iterative maximum a posteriori (IMAP)-DOAS for retrieval of strongly absorbing trace gases: model studies for CH_4 and CO_2 retrieval from near infrared spectra of SCIAMACHY onboard ENVISAT," Atmos. Chem. Phys. **5**, 9–22 (2005).
28. S. Oshchepkov, A. Bril, S. Maksyutov, and T. Yokota, "Detection of optical path in spectroscopic space-based observations of greenhouse gases: application to GOSAT data processing," J. Geophys. Res. **116**, D14304 (2011).
29. C. Cox and W. Munk, "Statics of the sea surface derived from sun glitter," J. Marine Res. **13**, 198–227 (1954).
30. C. D. Rodgers, *Inverse Methods for Atmospheric Sounding: Theory and Practice* (World Scientific, 2000).
31. A. Bril, S. Oshchepkov, and T. Yokota, "Application of a probability density function-based atmospheric light-scattering correction to carbon dioxide retrievals from GOSAT oversea observations," Remote Sens. Environ. **117**, 301–306 (2012).
32. H. Ishida and T. Y. Nakajima, "Development of an unbiased cloud detection algorithm for a spaceborne multispectral imager," J. Geophys. Res. **114**, D07206 (2009).
33. D. Wunch, G. C. Toon, P. O. Wennberg, S. C. Wofsy, B. Stephens, M. L. Fisher, O. Uchino, J. B. Abshire, P. F. Bernath, S. C. Biraud, J.-F. L. Blavier, C. D. Boone, K. P. Bowman, E. V. Browell, T. Campos, B. J. Connor, B. C. Daube, N. M. Deutscher, M. Diao, J. W. Elkins, C. Gerbig, E. Gottlieb, D. W. T. Griffith, D. F. Hurst, R. Jiménez, G. Keppel-Aleks, E. A. Kort, R. Macatangay, T. Machida, H. Matsueda, F. L. Moore, I. Morino, S. Park, J. Robinson, C. M. Roehl, Y. Sawa, V. Sherlock, C. Sweeney, T. Tanaka, and M. A. Zondlo, "Calibration of the Total Carbon Column Observing Network using aircraft profile data," Atmos. Meas. Tech. **3**, 1351–1362 (2010).
34. N. M. Deutscher, D. W. T. Griffith, G. W. Bryant, P. O. Wennberg, G. C. Toon, R. A. Washenfelder, G. Keppel-Aleks, D. Wunch, Y. G. Yavin, N. T. Allen, J.-F. L. Blavier, R. Jiménez, B. C. Daube, A. V. Bright, D. M. Matross, S. C. Wofsy, and S. Park, "Total column CO_2 measurements at Darwin, Australia—site description and calibration against *in situ* aircraft profiles," Atmos. Meas. Tech. **3**, 947–958 (2010).
35. J. Messerschmidt, J. R. Macatangay, J. Notholt, C. Petri, T. Warneke, and C. Weinzierl, "Side by side measurements of CO_2 by ground-based Fourier transform spectrometry (FTS)," Tellus B **62**, 749–758 (2010).
36. D. Belikov, S. Maksyutov, V. Sherlock, S. Aoki, N. M. Deutscher, S. Dohe, D. Griffith, E. Kyro, I. Morino, T. Nakazawa, N. Notholt, M. Rettinger, M. Schneider, R. Sussmann, G. C. Toon, P. O. Wennberg, and D. Wunch, "Simulations of column-average CO_2 and CH_4 using the NIES TM with a hybrid sigma-isentropic ($\sigma - \theta$) vertical coordinate," Atmos. Chem. Phys. Discuss. **12**, 8053–8106 (2012).
37. T. Takemura, M. Egashira, K. Matsuzawa, H. Ichijo, R. O'ishi, and A. Abe-Ouchi, "A simulation of the global distribution and radiative forcing of soil dust aerosols at the Last Glacial Maximum," Atmos. Chem. Phys. **9**, 3061–3073 (2009).
38. D. York, N. Evensen, M. Martínez, and J. Delgado, "Unified equations for the slope, intercept, and standard errors of the best straight line," Am. J. Phys. **72**, 367–375 (2004).